Rare Metal Materials and Engineering
Volume 54, Issue 6, June 2025
Available online at www.rmme.ac.cn

Science Press

Cite this article as: Wang Rui, Li Jiarong, Yue Xiaodai, et al. Deformation and Fracture Mechanism of Third-Generation Single Crystal Superalloy During In-situ Tension at Room Temperature[J]. Rare Metal Materials and Engineering, 2025, 54(06): 1410-1416. DOI: https://doi.org/10.12442/j.issn.1002-185X.20240291.

ARTICLE

Deformation and Fracture Mechanism of Third-Generation Single Crystal Superalloy During In-situ Tension at Room Temperature

Wang Rui, Li Jiarong, Yue Xiaodai, Zhao Jinqian, Yang Wanpeng

Science and Technology on Advanced High Temperature Structural Materials Laboratory, Beijing Institute of Aeronautical Materials, Beijing 100095, China

Abstract: The deformation and fracture of a third-generation single crystal superalloy during in-situ tension at room temperature were investigated at multiple scales by scanning electron microscope, electron back-scattered diffractometer, and transmission electron microscope to reveal the deformation and fracture mechanism during tension. The proportion of low angle boundaries (LABs) with angles from 2.5° to 5.5° increases during tension. The change in LABs is particularly pronounced after elongation over 7%. The initiation of microcracks is caused by {111}<110> slip systems. After initiation, the crack size along the stress direction increases whereas the size extension along slip systems is suppressed. The fracture mode of the alloy is quasi-cleavage fracture and the slip lines near the fracture are implicit at room temperature.

Key words: single crystal superalloy; in-situ tension; microstructure; slip system; fracture

1 Introduction

Ni-based single crystal superalloys are widely used in advanced aero-engines as turbine blades materials due to their excellent comprehensive properties[1–3]. Mechanical properties of single crystal superalloys are significant for turbine blades. Therefore, it is of great significance to research the deformation and fracture mechanism of single crystal superalloys under external load for the development and application of advanced aero-engines.

Heretofore, research on the deformation and fracture mechanism on single crystal superalloys under external load is mostly conducted after mechanical tests[4–11], namely ex-situ analysis, where researchers can only acquire the process of deformation and fracture during mechanical tests by inference. To analyze the deformation and fracture in real time under external load and to achieve more accurate mechanism of deformation and fracture of single crystal superalloys, many researchers pay attention to the in-situ research. Zhou et al[12] studied the impact of hole diameter on the tensile properties of DD33 alloy by analyzing the strain distribution around holes during in-situ tension at room temperature of the alloy with holes of different diameters (0.5 – 0.9 mm). Zhang et al[13] studied the effects of the structure of cooling holes on the tensile behavior of a single crystal superalloy using in-situ tension test. Ma et al[14] conducted an in-situ tension test at high temperature on a second-generation single crystal superalloy to obtain the microstructure evolution and fracture mechanism. Liu et al[15] analyzed the microstructure evolution of single crystal superalloy with different composition under in-situ tension at room temperature to study the influence mechanism of Re and Ru on tensile fracture mechanism of the alloys. Zhang et al[16] analyzed the microstructure evolution, including grain boundaries, grain orientations, and texture, by in-situ electron back-scattered diffraction (EBSD) during tension test of nickel-based superalloys. Ding et al[17] analyzed the mechanism of Re influence on the properties of single crystal superalloy under tensile stress by in-situ scanning electron microscope (SEM) and transmission electron microscope (TEM) analyses. Guo et al[18] investigated the effects of secondary orientation and temperature on the

Received date: May 16, 2024
Corresponding author: Li Jiarong, Ph. D., Professor, Science and Technology on Advanced High Temperature Structural Materials Laboratory, Beijing Institute of Aeronautical Materials, Beijing 100095, P. R. China, Tel: 0086-10-62497202, E-mail: jrli126@126.com

evolution of slip bands of a single crystal superalloy in in-situ tension test and proposed a model to simulate slip band evolution. Gupta et al[19] studied the relationship between plastic heterogeneity and crystal orientation of superalloys during in-situ tension tests using digital image correlation. The third-generation single crystal superalloy is a key material for advanced aero-engine turbine blades. However, the deformation and fracture mechanisms of the third-generation single crystal superalloy are rarely reported.

In this research, a third-generation single crystal superalloy was studied through in-situ tension at room temperature. The evolution of microstructures and microcracks of the alloy under tensile stress was investigated.

2 Experiment

The composition of the third-generation single crystal superalloy used in this research was 3.5Cr-7Co-2Mo-6.5W-7.5Ta-4.5Re-0.5Nb-5.6Al-0.1Hf-0.008C-0.001Y-Ni (wt%) [3]. The single crystal test plates of 100 mm×40 mm×10 mm were produced by the seed crystal method in an investment casting mold. The schematic diagram of test plate is shown in Fig. 1. Standard heat treatment (pre-treatment+1340 °C/6 h/air cooling +1140 °C/6 h/air cooling+870 °C/32 h/air cooling) was conducted on the as-cast test plates, and then the samples for in-situ tension tests were cut from the heat-treated test plates.

The size of sample for in-situ SEM and EBSD analyses is shown in Fig. 2. The surface was chemically corroded before the tensile test by 10vol% $HClO_4$ ethanol solution. In-situ SEM and EBSD analyses were conducted at room temperature with the loading rate of 20 N/s by SEM Zeiss Sigma 300 with an in-situ tension tester to analyze microstructure evolution, initiation and propagation of microcracks, as well as the evolution of low angle boundaries (LABs) of the third-generation single crystal superalloy during tension process. The map of grain boundary within a fixed region was measured using in-situ EBSD during the tensile process, and the angles of grain boundary were statistically analyzed from the map data. Grain boundary data were obtained at a certain deformation degree.

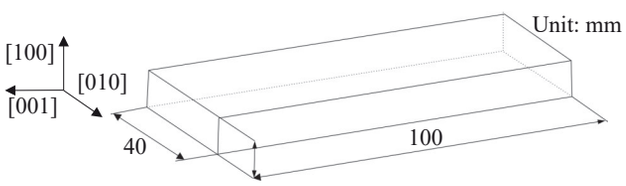

Fig.1 Schematic diagram of test plate

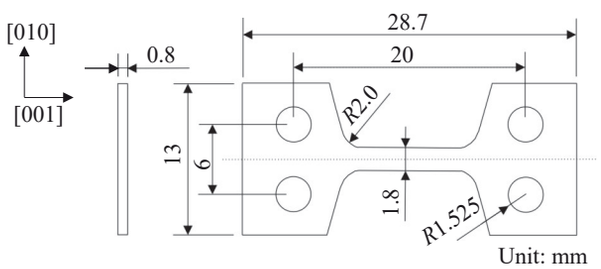

Fig.2 Schematic diagram of sample for in-situ SEM and EBSD analyses

The size of the sample prepared by focused ion beam (FIB) with two tensile working sections for in-situ TEM analysis is shown in Fig. 3. In-situ TEM was conducted with the loading condition of 2 nm/s at room temperature by TEM Talos F200X G^2 to study crack initiation and fracture mechanism.

3 Results

3.1 Tensile property

The stress-strain curve of in-situ tension at room temperature for the superalloy is shown in Fig. 4, and the property results are shown in Table 1.

The in-situ tension is a displacement-controlled process, which lasts for 774 s. The process for in-situ tension is as follows: obvious yielding occurs after elastic deformation, and then the stress increases continuously (stable plastic deformation) until fracture. The stress relaxation phenomenon occurs during the pause for SEM observation, resulting in the change points in the stress-strain curve. It can be seen that the in-situ tensile properties in this research are comparable to the conventional test results of other single crystal superalloys[20–21].

3.2 Microstructure evolution

Fig. 5 shows the surface evolution of the superalloy under different elongations during in-situ tension. When the

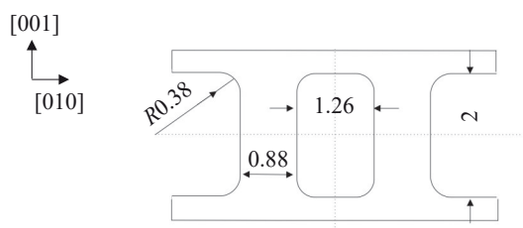

Fig.3 Schematic diagram of sample for in-situ TEM analysis

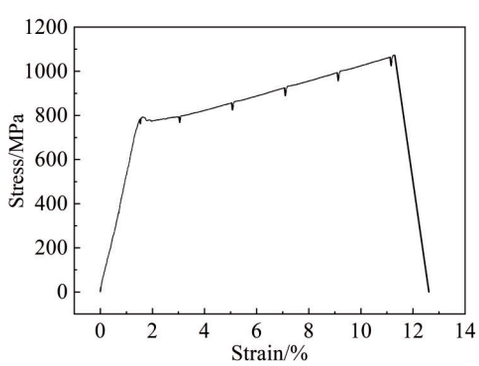

Fig.4 Stress-strain curve of superalloy during in-situ tension at room temperature

Table 1 In-situ tensile properties of superalloy (MPa)

Upper yield strength	Lower yield strength	Tensile strength
792	773	1073

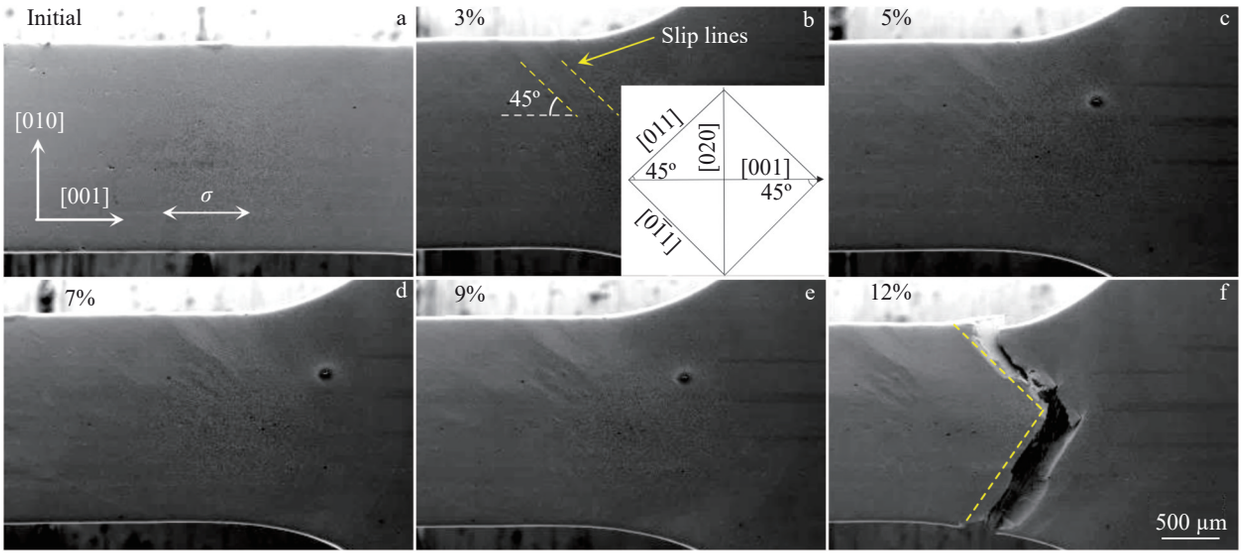

Fig.5 Surface evolution of superalloy under different elongations during in-situ tension: (a) initial, (b) 3%, (c) 5%, (d) 7%, (e) 9%, and (f) 12% (the inset in Fig.5b shows the projection of octahedral slip system on (100) plane)

elongation of the sample reaches 3%, a few slip lines with an angle of 45° to the stress direction with [001] orientation at the initial state occur. The slip lines are along {111}<110> slip systems, as shown in the inset of Fig. 5b. In addition, no obvious necking can be observed during tension, suggesting that the deformation of the entire sample is relatively uniform. The fracture direction (Fig. 5f) is consistent with the direction of the slip system. A similar fracture morphology can be observed in other alloys[15].

LAB is a kind of crystal defect in single crystal superalloys. LABs exceeding a certain degree can affect the mechanical properties of alloys[22–23]. Fig. 6 shows the evolution of the grain boundary angle of the superalloy during tension. The angles of LABs in the initial state are mainly 1.5° . The proportion of LABs of 1.5° decreases, whereas the proportion of LABs of 2.2°–5.5° increases slightly during tension. This change is particularly pronounced after elongation over 7%, which indicates a non-uniform local rotation of orientation in the sample during tension.

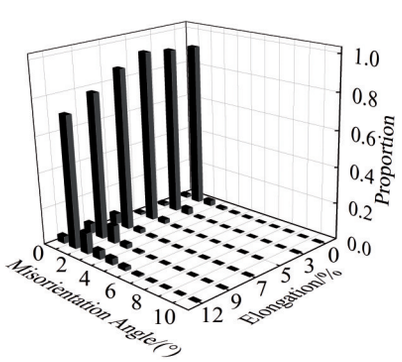

Fig.6 Misorientation angle distributions of LABs in superalloy under different elongations

3.3 Initiation and propagation of microcracks

Initiation and propagation of microcracks are the key processes that are directly related to the deformation and fracture of single crystal superalloys. Fig. 7 shows the initiation and propagation of microcracks during in-situ tension. Microcracks are mainly initiated at the edge of micropores, as shown in Fig. 7a$_1$. Several microcracks can be initiated from one single micropore. The initiation of microcracks occurs along the slip systems, as shown in Fig. 7a$_1$ and 7b$_1$. After initiation, the microcrack size along the stress direction increases whereas the size extension along slip systems is suppressed. In addition, slip lines can be observed at the crack tips.

Liu et al[15] found that a microcrack formed at the intersection of two sets of slip lines in a Ni-Al model single crystal superalloy. The observed microcrack presents two crack tips resulting from the coupling effect of two different slip systems. The microcrack in this research has only one certain crack tip because no coupling effect of different slip systems occurs during the initiation of cracks.

TEM analysis of the superalloy during in-situ tension at room temperature was conducted to further study the initiation and propagation of microcracks. Fig. 8 and Fig. 9 show the initiation and propagation of microcracks. In Fig. 8a–8b, two slip bands with an angle of 70° can be observed, and each slip band presents an angle of 35° to [001] orientation (stress direction), which infers that the microcrack is along {111}<110> slip systems, as shown in Fig. 8c. Additionally, cross slip occurs during the microcrack initiation.

Fig.9 shows the fracture morphologies and the propagation path of microcracks of TEM samples after in-situ tension. It can be seen that the fracture morphologies of the two working sections are similar despite the difference in fracture positions in the sample. The crystallographic planes are

serrated with an angle of 70°.

3.4 Fracture

Fig. 10 shows the fracture morphologies of the superalloy after in-situ tension. It can be seen that the fracture is roughly composed of two planes. A large number of crystallographic planes can be observed. The fracture morphology shows the characteristics of quasi-cleavage fracture, which is composed of crystallographic planes.

4 Discussion

LABs occur inevitably in the preparation process of single crystal superalloys[24]. There are a certain number of LABs with an angle of 1.5° in the superalloy used in this study. The orientation difference between both sides of LAB causes the inequality in the Schmidt factor[25] within local regions, leading to a relative rotation that increases the angles of LABs. Hence, the proportion of LABs of 2.2°–5.5° increases, as shown as in Fig. 6. The region of relative rotation is increased with further tension because of the enhancement in tensile stress. Besides, the increase in the proportion of LABs of 2.2°–5.5° is more evident after elongation over 7%.

There is usually a certain degree of stress concentration at the crack tip due to the sudden change in the cross-section, which results in a plastic deformation zone within a certain range at the crack tip to alleviate the stress concentration[26]. Slip lines at the crack tips in Fig.7 indicate the occurrence of plastic deformation. The plastic deformation reduces stress concentration, restraining the further microcrack propagation along the slip lines. However, the initiated microcracks are pulled laterally under external stress, evolving into the morphology in Fig. 7. This microcrack propagation mode of the superalloy contributes to the uniform deformation in Fig.5. The universality of the microcrack propagation mode may result in the fine elongation, as shown in Fig.4.

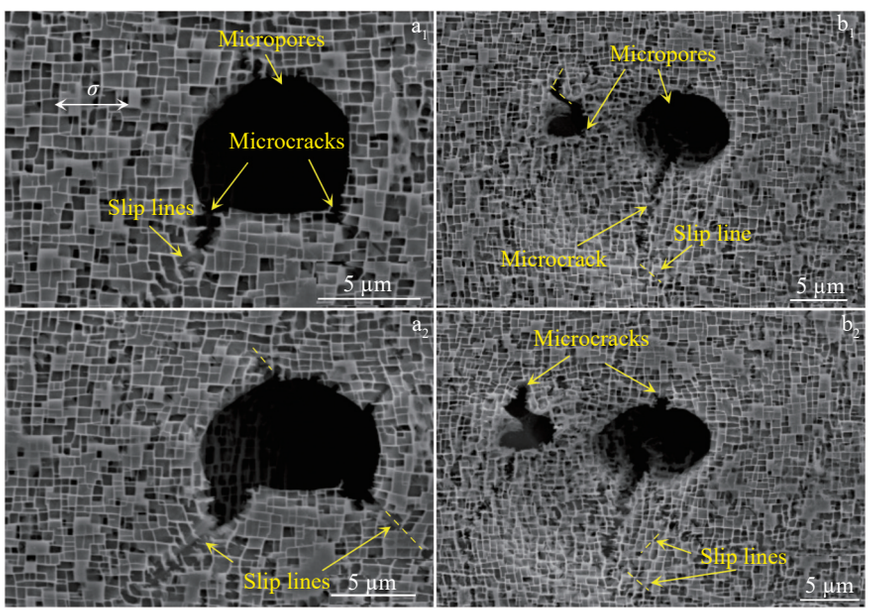

Fig.7 Initiation and propagation of microcracks during in-situ tension: (a_1, b_1) microcrack at elongation of 3%; (a_2, b_2) microcrack after fracture

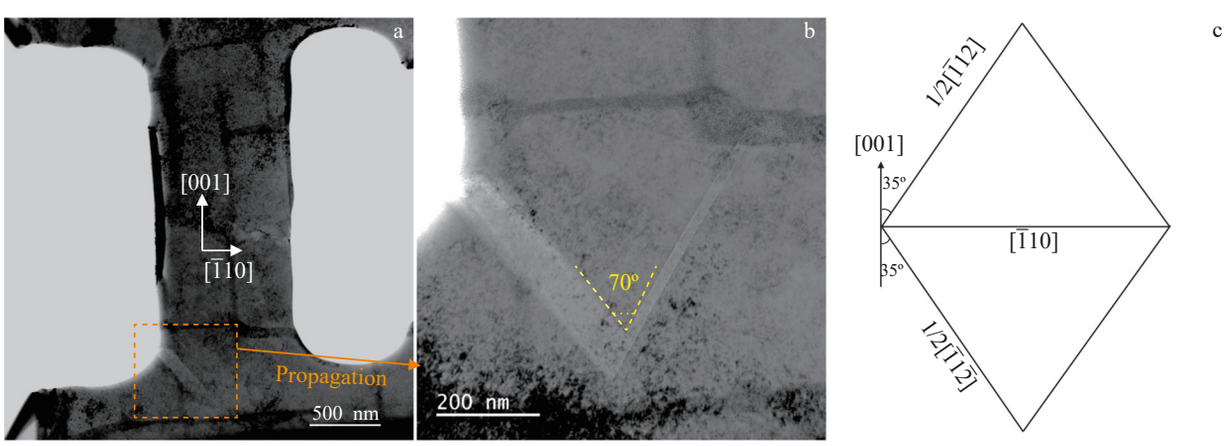

Fig.8 TEM images of microcrack initiation and propagation with zone axis of [110] (a–b); projection of octahedral slip system on (110) plane (c)

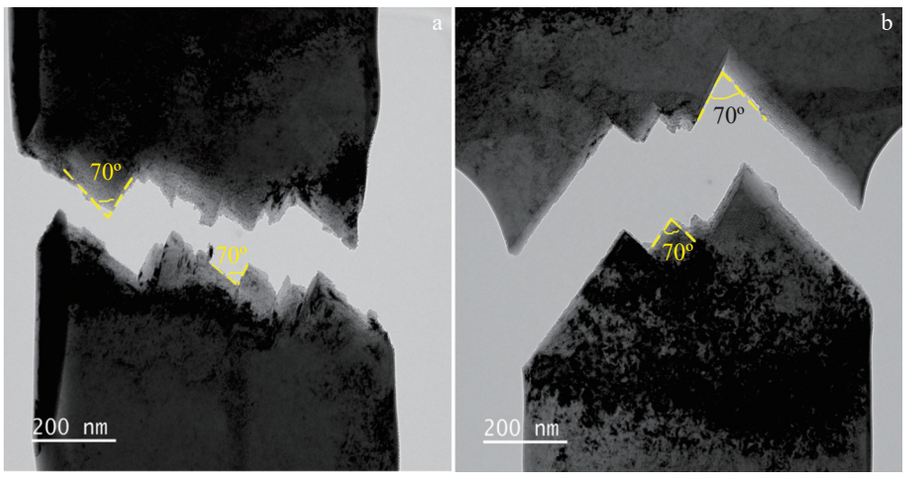

Fig.9 TEM fracture morphologies of superalloy after in-situ tension with zone axis of [110]

There is a competitive relationship between slip and cleavage[27] during the tensile deformation of single crystal superalloys. As shown in Fig. 10, the fracture shows the characteristics of cleavage. However, slip characteristics are observed throughout the whole tensile process. When the cracks propagated on different slip planes meet each other, the step morphology in Fig. 10c – 10d can be observed. Furthermore, the superalloy presents fine plasticity, according to Fig.4. Therefore, the fracture mode for tension at room temperature of this superalloy is quasi-cleavage mode.

The fracture characteristics of the alloy in this study are similar to those of other alloys[15,28] during in-situ tension at room temperature. However, slip lines can barely be observed near the fracture area of the superalloy, which is significantly different from the massive slip lines near the fracture region of the third-generation single crystal superalloy DD33 with a preset hole, as shown in Fig. 11[28]. The preset hole with a diameter of 5 mm was obtained by drilling on a smooth sample in the middle of the gauge length to investigate the tensile behavior of the alloy with a preset hole[28]. The preset hole induced obvious stress concentration. Furthermore, necking phenomenon occurred near the preset hole and finally resulted in fracture (Fig. 11). Therefore, in this study, the relative uniform deformation in the smooth superalloy leads to implicit slip lines and necking phenomenon near the fracture (Fig.5f and Fig.10b).

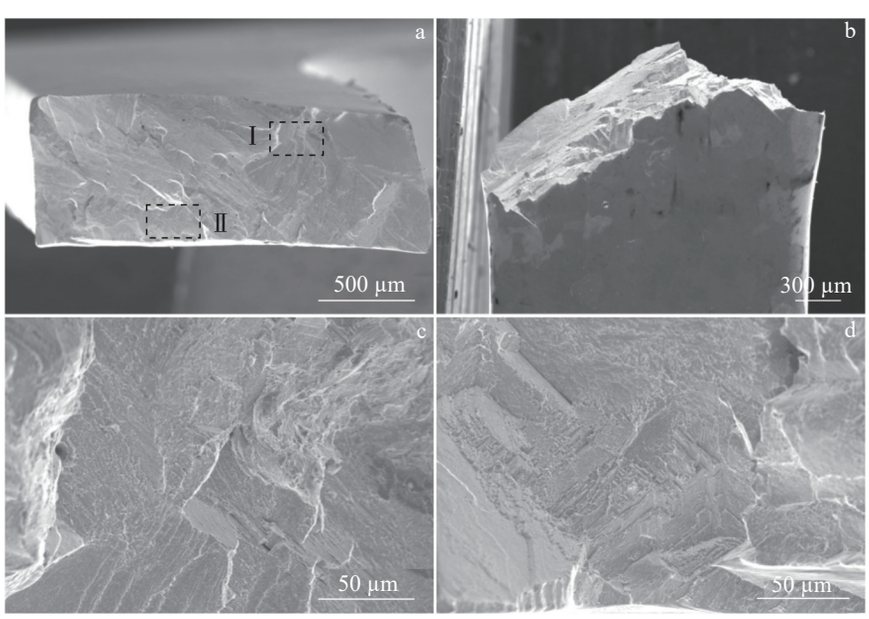

Fig.10 Fracture morphologies of superalloy after in-situ tension: (a–b) overall fracture morphologies; (c) enlargement of region I in Fig. 10a; (d) enlargement of region II in Fig.10a

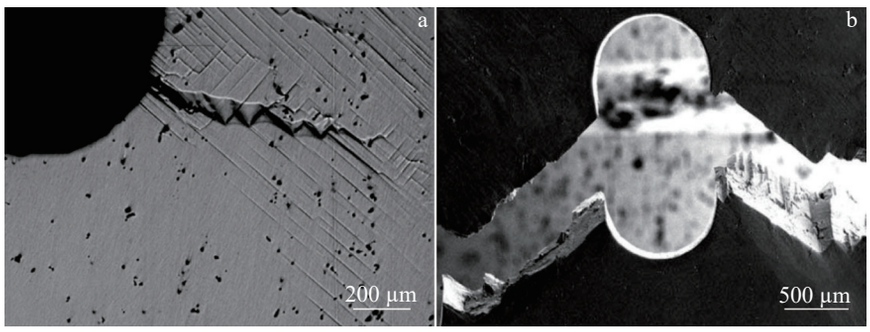

Fig.11 In-situ tension test results of DD33 alloy with a preset hole[28]

5 Conclusions

1) The proportion of LABs with the angle from 2.5° to 5.5° increases during tension, and the increment is particularly pronounced after elongation over 7%.

2) The microcracks are initiated along {111}<110> slip systems. After initiation, the microcrack size along the stress direction increases, whereas the size extension along slip systems is suppressed by the slip near the crack tips. The propagation mode of microcracks is one of the reasons contributing to the fine plasticity of the superalloy.

3) The fracture mode of superalloy after tension at room temperature is quasi-cleavage mode. The deformation of the superalloy is relatively uniform during tension.

References

1 Duhl M G D N, Giamei A F. *Superalloys*[J], 1980, 41: 205

2 Harris K, Erickson G L, Sikkenga S L *et al. Journal of Materials Engineering and Performance*[J], 1992, 2(4): 481

3 Li Jiarong, Liu Shizhong, Wang Xiaoguang *et al. Superalloys 2016: Proceedings of the 13th International Symposium of Superalloys*[C]. Seven Springs: The Minerals, Metals & Materials Society, 2016: 57

4 Wang Jianjun, Guo Weiguo, Li Penghui *et al. Materials Science & Engineering A*[J], 2016, 670: 1

5 Shi Zhenxue, Liu Shizhong, Yue Xiaodai *et al*. *Rare Metal Materials and Engineering*[J], 2022, 51(10): 3542

6 Zeng Qiang, Chen Xuhui, Wu Baoping *et al*. *Rare Metal Materials and Engineering*[J], 2022, 51(9): 3394 (in Chinese)

7 Shi Zhenxue, Liu Shizhong, Yue Xiaodai *et al*. *Rare Metal Materials and Engineering*[J], 2023, 52(6): 1977

8 Yang Wanpeng, Li Jiarong, Liu Shizhong *et al*. *Rare Metal Materials and Engineering*[J], 2018, 47(10): 2964 (in Chinese)

9 Cervellon A, Hémery S, Kürnsteiner P *et al. Acta Materialia*[J], 2020, 188: 131

10 Zhang Peng, Yuan Yong, Gao Zhenhuan *et al. Journal of Alloys and Compounds*[J], 2021, 862: 158478

11 Tang Y T, D'Souza N, Roebuck B *et al. Acta Materialia*[J], 2021, 203: 116468

12 Zhou Zhongjiao, Liu Tao, Zhang Gong *et al. Chinese Journal of Materials Research*[J], 2016, 30(5): 343 (in Chinese)

13 Zhang Zhanfei, Wang Wenhu, Jiang Ruisong *et al. International Journal of Mechanical Sciences*[J], 2022, 229: 107514

14 Ma Jinyao, Wang Jin, Zhao Yunsong *et al. Acta Metallurgica Sinica*[J], 2019, 55(8): 987 (in Chinese)

15 Liu Chengpeng, Zhang Xiaona, Ge Lin *et al. Materials Science & Engineering A*[J], 2017, 682: 90

16 Zhang Chao, Ya Ruhan, Sun Ming *et al. Materials Today: Communications*[J], 2023, 35: 105522

17 Ding Qingqing, Li Suzhi, Chen Longqing *et al. Acta Materialia* [J], 2018, 154: 137

18 Guo Zixu, Song Ziyuan, Ding Xin *et al. International Journal of Plasticity*[J], 2023, 165: 103600

19 Gupta R, Sharma V, Prasad M J N V *et al. Materials Science & Engineering A*[J], 2023, 880: 145310

20 Liu Jinlai, Yu Jinjiang, Jin Tao *et al. Transactions of Nonferrous Metals Society of China*[J], 2011, 21(7): 1518

21 Tan Zihao, Wang Xinguang, Du Yunling *et al. Materials Science & Engineering A*[J], 2020, 776: 138997

22 Zhao Jinqian, Li Jiarong, Liu Shizhong *et al. Rare Metal Materials and Engineering*[J], 2007, 36(12): 2232 (in Chinese)

23 Li Huifen, Liu Lijun, Xue Ming *et al. Materials Science Forum* [J], 2017, 898: 498

24 Li Jiarong, Xiong Jichun, Tang Dingzhong. *Advanced High Temperature Structural Materials and Technology*[M]. Beijing: National Defense Industry Press, 2012 (in Chinese)

25 Jiang Wexiang, Lu Junxia, Li Feiqi *et al. Materials Science & Engineering A*[J], 2022, 849: 143453

26 Liang Jiecun, Wang Zhen, Xie Hongfu *et al. International Journal of Fatigue*[J], 2019, 128: 105195

27 Zhong Qunpeng, Zhao Zihua. *Fractography*[M]. Beijing: Higher Education Press, 2006 (in Chinese)

28 Zhou Zhongjiao, Wang Li, Wang Dong *et al. Materials Science & Engineering A*[J], 2016, 659: 130

第三代单晶高温合金室温原位拉伸变形及断裂机理

王　锐，李嘉荣，岳晓岱，赵金乾，杨万鹏

(北京航空材料研究院 先进高温结构材料重点实验室，北京 100095)

摘　要：采用扫描电子显微镜、电子背散射衍射和透射电子显微镜对一种第三代单晶高温合金在室温原位拉伸过程中的变形和断裂进行了多尺度研究，揭示了拉伸过程中的变形和断裂机制。在拉伸过程中，角度为2.5°~5.5°的小角度晶界(LAB)的比例增加，并且LAB的增加在伸长率超过7%之后尤其明显。微裂纹的萌生是由{111}<110>滑移系引起的，微裂纹萌生后，沿应力方向的尺寸增加，而沿滑移系方向的尺寸扩展受到抑制。合金为类解理断裂，断口附近的滑移线并不明显。

关键词：单晶高温合金；原位拉伸；微观组织；滑移系；断口

作者简介：王 锐，男，1994年生，博士生，北京航空材料研究院先进高温结构材料重点实验室，北京 100095，电话：010-62498309，E-mail：WR0608@126.com